

# **Radiation risk assessment for space applications by using PW laser facilities**

A. Groza<sup>1</sup>, E. Stancu<sup>3,6</sup>, A. Chiroasca<sup>1,5</sup>, B. Butoi<sup>1</sup>, D.B. Dreghici<sup>1,5</sup>, M. Serbanescu<sup>2,7</sup>,  
C. Ticos<sup>4</sup> and M. Ganciu<sup>1\*</sup>

<sup>1</sup> National Institute for Laser, Plasma and Radiation Physics (INFLPR), Low Temp. Plasma Dept., Atomistilor Str. No. 409, 077125 Magurele, Ilfov County, Romania

<sup>2</sup> National Institute for Laser, Plasma and Radiation Physics, Centre for Advanced Laser Technology (CETAL-PW), Atomistilor Str. No. 409, 077125 Magurele, Ilfov County, Romania

<sup>3</sup> National Institute for Laser, Plasma and Radiation Physics, STARDOOR Dept., Atomistilor Str. No. 409, 077125 Magurele, Romania

<sup>4</sup> National Institute for Laser, Plasma and Radiation Physics (INFLPR), Accelerator Dept., Atomistilor Str. No. 409, 077125 Magurele, Ilfov County, Romania

<sup>5</sup> Faculty of Physics, University of Bucharest, Nuclear Phys. Dept. Magurele, Romania

<sup>6</sup> Faculty of Physics, University of Bucharest, Doctoral School in Physics, Magurele, Romania

<sup>7</sup> Politehnica University of Bucharest (UPB), Faculty of Electronics, Telecommunications and Information Technology Splaiul Independentei 313, Bucharest 060042, Romania

\* Correspondence: mihai.ganciu@inflpr.ro;

## **Abstract**

The map of the radiation doses inside a target chamber during a high-power laser - thin solid target experiments is experimentally measured and theoretically calculated. Maximum values for the integrated doses per laser shot of around tens of mGy per shot are obtained in a direction normal to the target, at a distance of about 30 cm from the laser-target interaction point. The simulated map of the radiation doses around the high-power laser thin foil interaction point is obtained by using the Geant 4 General Particle Source code and the geometry of the experimental setup. The computed radiation doses map present similarities with the experimental doses map.

**Keywords:** radiation-hardening; critical infrastructures; space radiations; radiation effects; laser-plasma accelerators; radiation hardness testing.

## **1. Introduction**

Space weather is the name given to a series of phenomena which occur in the Solar System, and especially around the Earth, due to the influence of the Sun. Its changing and complex nature, as well as its dependence on the Sun, makes it somewhat similar to terrestrial weather, but the physics involved is generally totally different. The concept of space weather can be described as the time-variable conditions in the Sun, solar wind, magnetosphere, thermosphere and ionosphere that can affect space-borne or ground-based technological systems and might threaten human life. Due to these destructive effects, in order to protect the Earth, we need to understand these causes [1].

Apart from some influences outside the Solar System, space weather has its origin in the Sun. The space weather system around the Earth consists of solar wind, Sun, solar magnetic field, magnetosphere and ionosphere. Although the Sun is continuously emitting a supersonic plasma flow called solar wind that forms a bubble in the interstellar medium known as the heliosphere, it also releases huge amounts of matter [1-4]. Large magnetic storms are created in the magnetosphere and the upper atmosphere as a result of the matter generated from the Sun directed towards Earth.

While the Sun's output in optical and near-infrared radiation is quite constant, there is significant variability, particularly during solar storms, in the output of EUV (extreme ultraviolet), X-ray and radio waves. At these times, the Sun also generates high-energy solar energetic particles (SEPs), while the solar wind plasma, which comes from the solar corona, increases in speed and density. Coronal mass ejections (CMEs) constitute an example of this phenomenon. In addition to this, stream interaction regions (SIRs) also appear when fast streams in the solar wind overtake and compress slower streams [1-4].

The ionizing radiation, the ionized particles and the plasma interact with the magnetosphere or the ionosphere either directly or indirectly, which can potentially cause damage to engineering systems. These effects depend on the orientation of the heliosphere magnetic field (HMF) usually referred to the interplanetary magnetic field (IMF) that controls the way in which CMEs and SIRs can influence the magnetosphere-ionosphere system producing disturbances called geomagnetic storms [3]. The geomagnetic storms are the disturbances on the Earth magnetosphere caused by the interaction between the solar magnetic fields pulled out from the solar corona and carried into interplanetary space by the solar wind and the Earth's magnetic field.

Although the Earth is protected from the solar weather by its magnetic field and atmosphere, when the IMF has a component which points to the south, magnetic reconnection between the IMF and the Earth's magnetic field occurs on the dayside of the magnetosphere, which allows the solar wind to enter the magnetosphere [1-4]. In this case, the solar event is called geoeffective. Another effect of the solar weather happens when the energy from the solar wind is transported to the other side of the Earth and stored in the tail of the magnetosphere until it reaches a critical level. At that point, the energy is released explosively through a phenomenon called magnetic reconnection and part of it is directed towards the Earth. This process (storing energy then suddenly releasing it) is known as a sub storm and occurs while solar wind energy enters the magnetosphere producing the well-known northern and southern auroral lights.

In order to prevent the disturbances coming from outside the Earth system, especially the ones that starts at the Sun it is indispensable to recognize and prevent the effects that originate at the base of space weather. In recent years, the most important studies related to space weather are in the spacecraft research field. Due to the penetration of high energy particles through the spacecraft material, major damages can be caused in the spacecraft electronics or software [2, 3].

Spacecraft charging, the accumulation of an electrostatic charge on the non-conducting materials on the spacecraft's surface by low energy particles is one of the predominant space weather effects on a spacecraft in the orbit [4]. Another harmful effect would be the exposure of the human body to the space radiation (ionizing radiation) [4, 5]. Preliminary results obtained in our laboratory have shown that simple electronic circuits introduced in the electron beam obtained from an electron accelerator were rendered inoperable after an irradiation time of only a few seconds, to a dose ~100-300 Gy. The beam energy was 6 MeV [6].

Similar conditions to those found in the environment of space stations and spacecraft can be obtained using high power lasers [7]. High intensity lasers have progressively been used in nowadays research for the study of matter under extreme conditions such as particle accelerations. The plasma created on the surface of the target, as a result of high intensity laser-matter interactions in vacuum, and the interactions between the plasma and the laser pulse can accelerate the plasma electrons up to tens of MeV [7, 8, 9]. The “hot” electrons and laser accelerated electrons interact with the target chamber walls generating X - ray bremsstrahlung photons. The mixed field of photons and electrons might create a radiation hazard associated with such laser-matter interactions experiments [7].

Thus, different ionizing particle types and doses can be obtained in high power laser - thin solid target experiments. For example, protons with energies up to tens of MeV and mixed fields of electrons and photons with doses of tens of mGy/per laser shot, depending on the target thickness and material type, can be generated [8]. These experimental conditions can be obtained in high power lasers-solid target experiments that can be performed at high power laser facilities available now [10, 11, 12].

The experiments performed and reported in this paper mimic the radiation dose characteristic to interiors and exterior of space stations and spacecraft cabins. Such experiments are very useful for radiation hardness testing of electronics and software. In the past, [13], the aspects of radiation hardness testing of the electronic systems find outside space stations and spacecraft cabins were largely discussed.

In this paper we measured the integrated doses produced by the mixed field of electrons and X-ray photons generated during high power laser-thin solid targets interaction experiments in which laser accelerated protons with energy about 14 MeV [14] were demonstrated by using CETAL high power laser facility [11].

## **2. Materials and methods**

### *2.1 Experimental set-up*

The mapping of the radiation dose inside the target chamber has been performed during experiments of high power-thin solid target interaction for a laser intensity in focus of about  $5 \times 10^{19} \text{ W/cm}^2$  (40 fs pulse duration [15]). The laser incidence angle with respect to the target normal was  $45^\circ$ . The laser spot surface area was about  $(9 \times 23) 207 \mu\text{m}^2$  and the fraction of energy in the laser spot (at full width half maximum) was  $\sim 30\%$ .

Dose assessment was performed with passive detectors – CR-39 [14] and radiochromic films, while the dose map inside the interaction chamber was estimated using radiation transport software (GEAN4 v. 10.5). The experimental set-up from Figure 1 was designed in order to allow a straightforward analysis of laser accelerated electron and proton beams. It is composed of the targets and passive detectors holder ensemble, a magnetic spectrometer, and an optical analysis ensemble. The magnetic spectrometer was used for estimation of electron beam energy. The target and detector holder system consist in two parallel metallic plates centered using a horizontal metallic axis. The targets are positioned on the first plate while the passive detectors used for proton beams analysis are mainly placed on the second plate. On the second plate, the passive detectors alternate with blank hole positions. Behind the second plate a centered magnetic spectrometer (used for the estimation of the energy of the electrons accelerated as result of high-power laser-solid target interaction) is fixed aligned with the beam propagation

direction (see Figure 1). The spectrometer is used for the estimation of the electrons energy, accelerated as a result of high-power laser-solid target interaction. Around the magnetic spectrometer a metallic cylinder is rotated. On the inner surface of the metallic cylinder (see Figure 1) the radiochromic films used for estimation of the laser accelerated electron energies ( $\sim 14$  MeV) are positioned.

The target and detector holder ensemble are placed on mechanical translation and rotation stages for precise x-y-z alignment in the focus of the laser beam. The optical analysis system was described in details in [14].

Passive detectors within  $2 \times 2 \text{ cm}^2$  size of EBT3 radiochromic films were covered with aluminum foil of 10 microns thickness and placed inside the target chamber at different distances around the experimental set-up as presented in Figure 1. Thus, the integrated dose (mGy) generated from the mixed field of electrons and bremsstrahlung photons generated from high power laser-thin solid targets interaction experiments was also measured in our experimental configuration.

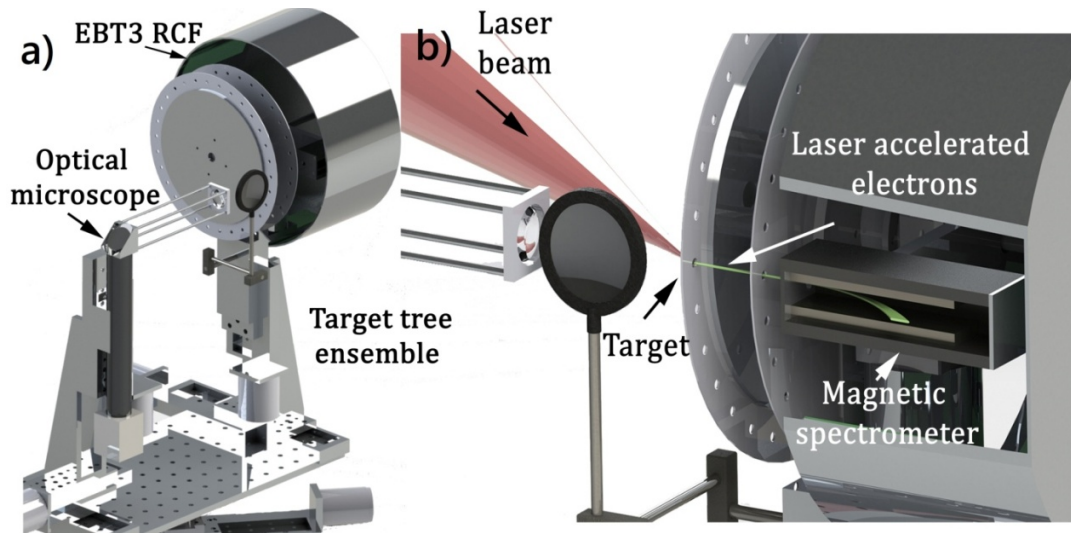


Figure 1: a) Experimental set-up; b) Detailed of the experimental set-up.

## 2.2 Method for dose estimation from radiochromic films

The dosimetry assessment during high power lasers-thin solid target interaction performed using the EBT3 radiochromic films is very useful and gives two-dimensional information of the radiation dose. The EBT3 films have a symmetrical layer's structure as the active layer ( $28 \mu\text{m}$  thick) is sandwiched between two  $125 \mu\text{m}$  matte-polyester substrates (Ashland Advanced Materials). These polyester layers prevent the formation of Newton ring interference patterns when the irradiated EBT3 films are scanned with flatbed scanners [16].

The EBT3 films irradiated during the high-power laser thin solid target experiments were scanned using an EPSON Expression 11000XL scanner with a resolution of 4800 dpi in transmission mode. The scanned area of each film was about  $0.5 \times 0.5 \text{ cm}^2$ . The scanned images were transformed into 8 bits grey scale and processed with ImageJ software in order to convert

the image pixels into standard optical density [17]. The calculation of the optical density of each irradiated film with high precision is essential for the finding of the exact values of the radiation doses inside the target chamber.

The EBT3 films were previously calibrated using 40 kV X-rays generated by an X ray source [18]. The dosimetry measurements have been performed using a plane parallel chamber connected to UNIDOS Secondary Standard Dosimeter, previously calibrated to PTB primary standard. Using the calibration graph presented in Figure 2 the radiation doses inside the target chamber was determined. The black points represent the measurements and the red curve is the fitting curve. The fitting parameters can be observed in the figure legend.

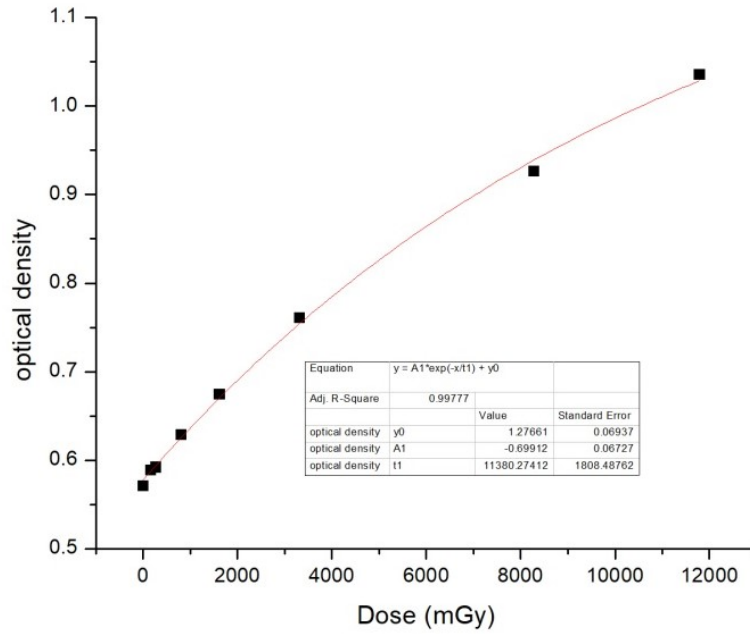


Figure 2: The dependence of optical density on radiation dose.

### 3. Results and discussions

#### 3.1 Experimental map of the measured doses inside the target chamber

The interaction of high-power lasers with thin solid targets generates fluxes of protons, electrons, X- ray radiation and neutrons of different energies [7, 19, 20]. The laser accelerated electrons that interact with the walls of the target chamber produce X-ray bremsstrahlung radiations [7].

In the experiments performed and described in the experimental section above, we map the radiation doses inside the target chamber. Figure 3 shows the map of the radiation dose measured inside the interaction chamber for a laser intensity of  $5 \times 10^{19} \text{ W/cm}^2$ . The dose values are per shot and were normalized to 30 cm distance.

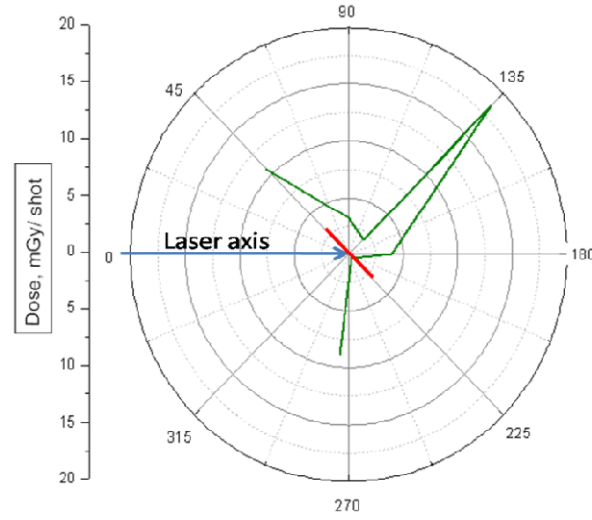


Figure 3: Map of measured doses per shot at 30 cm inside the target chamber for  $5 \times 10^{19} \text{ W/cm}^2$ .

In Figure 3 one can observe that the maximum values of the radiation doses were reached on a direction normal to target. The experiments of high-power laser- thin solid target interaction present the advantage of generating mixed radiation fields similar with the ones encountered inside spacecrafts and space station.

The values of the radiation doses per laser shot measured inside the target chamber during high power laser-thin solid target interaction are close with doses measured outside spacecrafts and space stations [14, 21- 26]. The knowledge of radiation field outside the spacecraft, is important to estimate the radiation field inside. In [22] mean measured values of hundreds of  $\mu\text{Gy}$  for cumulative radiation doses inside cabin spacecrafts by day were reported.

Inside the spacecrafts and space stations there are a lot of electronic systems and software preferable to be previously tested on Earth in dedicated facilities. That is why the testing and characterization of the detectors at ground-based facilities is important, in order to overcome the problems inherent in space dosimetry.

Thus, such radiation environment generated in high power laser-thin solid target experiments can simulate harsh space environment specific to space stations and spacecraft cabin habitats, important also for testing and optimization of different shielding materials [27].

### 3.2 Simulation model of the experimental radiation map

The experimental conditions allowed for the reconstruction of the radiation field within the target chamber lead to the description of specific radiation conditions (flow and dose) at any point within the interaction camera.

Dose reconstruction was performed by the means of radiation transport simulation using the Geant4 v.10.5 framework [28-30]. In order to obtain an appropriate simulation, two volume sources were considered.

The first source is the pre-plasma obtained after the interaction of the PW laser with the target surface ( $T_{\text{hot electrons}} = 2.8 \text{ MeV}$ ). Here relativistic electrons that were transported through the target up to detectors were generated. This source was considered to have uniform angular distribution and Gaussian energy distribution. The position of this source is chosen to be in front

of the target, on the opposite side with the pre-plasma [9, 31, 32]. In Figure 4a, the pre-plasma is illustrated as a yellow disk. The red disk (see Figure 4a) represents the target. The energy of the laser accelerated electrons was estimated to be around 17 MeV.

The second source in the simulations is the proton source that has a focused angular distribution along its normal to the surface behind the target. Considering the Target Normal Sheath Acceleration (TNSA) model [9, 19, 20] the spectral distribution of protons was extracted. It was obtained different values of proton energies function of the target thickness: 16.7 MeV for a 10  $\mu\text{m}$  Al target [23,33,34].

These two sources were implemented using Geant4 General Particle Source (that allows the positioning of more than one source within an experimental set-up) with a 10:1 partition for relativistic electron source with respect to the proton source. The mesh of the simulation geometry presented in Figure 4a, includes beside the proton and electron sources, the exact parameters of the experimental setup (see Figure 1). The protons propagating from the source through the environment produced nuclear reactions when interact with each component element of the experimental set up within the simulation area producing secondary radiations such as photons and electrons. The fluencies of the electrons and photons are presented in Figure 4b and 4c.

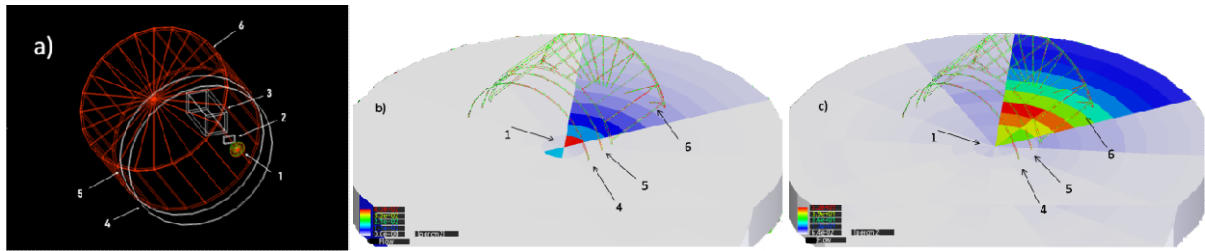


Figure 4: a) Geometry Mesh of the GEANT4 simulation: 1-sources of laser accelerated electrons and protons; 2- hole; 3-magnetic spectrometer; 4- target holder; 5- detector holder; 6-aluminium cylinder b) Simulated electron fluencies; c) Simulated photon fluencies.

The simulations performed using the mesh from Figure 4a were normalized according to the source distribution (mainly for the proton distribution leading to  $1.9 \cdot 10^7$  events in the target). The results were obtained using command line-based scoring for the laser plane within a 30 cm radius disk placed on the Z axis (the axis of proton and electron beam propagation) with 30-degree angle step. The simulated results presented in Figure 5 are in acceptable agreement with the experimental data presented in Figure 3.

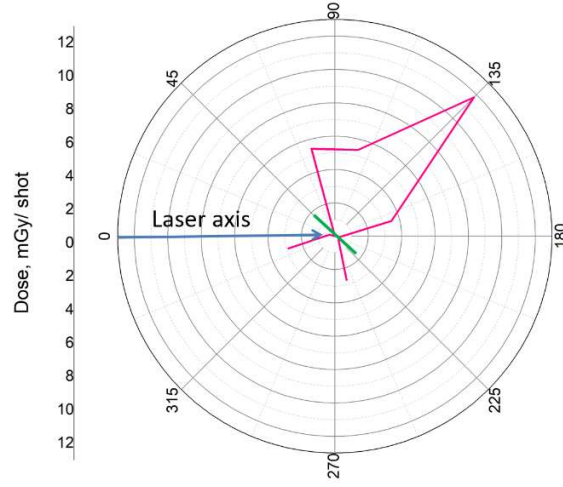


Figure 5: Map of the simulated radiation doses inside the target chamber.

Radiation transport simulations were calibrated with radiation dose values measured within the target chamber. It allows the radiation field reconstruction in any point within the area of interest around the experimental set-up. By using a calibration factor of about 1.4 we extract information about particle type, spectra and fluencies in different points within the target chamber.

Once the theoretical module was validated with experimental results, similar evaluations can be obtained using infinite sources (specific to the space like radiation environment) that better simulate the space environment. Such simulations can provide valuable input for spacecrafts shield design or for space radiation exposure assessment [25, 27, 35].

#### 4. Conclusions

We report in this paper the map of the radiation doses measured inside a target chamber during the experiments of laser proton acceleration using thin solid targets. We estimated that the maximum energy of the protons during the performed experiments was about 13.8 MeV.

Integrated dose (of mixed radiation fields of electrons and photons) per laser shot of about 15 mGy in the normal direction to the target at 30 cm distance from the laser-target interaction point was performed. A mesh of the experimental set-up geometry was generated and used as input for the calculation of the radiation doses around the high-power laser - solid thin foil interaction point, using Geant4 General Particle Source code. The obtained radiation doses map indicated similar values with the measured one.

The experimental and simulated results presented in this paper suggest that high power laser-thin solid target experiments can be used as test environment for electronics and software equipment used in spacecraft and space station habitats.

For the particular geometry described here we find a good match between measurements and simulations. This finding validates the numerical simulations implemented by our code. We extend our assumption and claim that our code can also be used for other types of radiation sources to simulate radiation in and around space stations, at least by supposing a superposition of radiation fields, if no nonlinear effects occur. Generally, we agree that there is a big difference between the space radiation background and the one generated by solid-target laser interaction.



The first one is pseudo-continuous while the second one comes in short pulses. However, the key advantage of the laser-plasma interactions is that it can generate simultaneously protons, X-rays and electrons. The acceptable agreement between the experimental and simulated data obtained in this report, lead to possibility of applying the used simulation tools to characterize and simulate new shielding design materials of actual interest.

**Conflicts of Interest:** The authors declare no conflict of interest. The funders had no role in the design of the study; in the collection, analyses, or interpretation of data; in the writing of the manuscript, or in the decision to publish the results.

**Acknowledgments:** We acknowledge support from the CETAL-PW facility at the National Institute for Laser, Plasma and Radiation Physics, Magurele, Romania.

**Funding:** Work has been funded by European Space Agency within the ESA contract No.4000121912/17/NL/CBi by Romanian National Authority for Scientific Research and Innovation, contract No. 3N/2018 (Project PN 18 13 01 03) and by Romanian Space Agency, contract No. 53/19. 11. 2013 (Competence Center: Laser-Plasma Acceleration of Particles for Radiation Hardness Testing - LEOPARD)

## References

- [1] Holly Zell, National Aeronautics and Space Administration, Page Last Updated: Aug. 4, 2017, [https://www.nasa.gov/mission\\_pages/rbsp/science/rbsp-spaceweather.html](https://www.nasa.gov/mission_pages/rbsp/science/rbsp-spaceweather.html)
- [2] Tokumaru, M. (2013). Three-dimensional exploration of the solar wind using observations of interplanetary scintillation. *Proceedings of the Japan Academy, Series B*, 89(2), 67–79. <https://doi.org/10.2183/pjab.89.67>
- [3] Cannon, P. (2013). Extreme space weather: impacts on engineered systems and infrastructures. In *Royal Academy of Engineering*. Retrieved from [http://www.raeng.org.uk/news/publications/list/reports/Space\\_Weather\\_Full\\_Report\\_Final.PDF](http://www.raeng.org.uk/news/publications/list/reports/Space_Weather_Full_Report_Final.PDF)
- [4] Delzanno, G. L., Borovsky, J. E., Thomsen, M. F., Moulton, J. D., & Macdonald, E. A. (2015). Future beam experiments in the magnetosphere with plasma contactors: How do we get the charge off the spacecraft? *Journal of Geophysical Research: Space Physics*, 120(5), 3647–3664. <https://doi.org/10.1002/2014JA020608>
- [5] Holly Zell, National Aeronautics and Space Administration, Page Last Updated: Aug. 4, 2017, Holly Zell [https://www.nasa.gov/mission\\_pages/rbsp/science/rbsp-spaceweather-human.html](https://www.nasa.gov/mission_pages/rbsp/science/rbsp-spaceweather-human.html)
- [6] Ticoș, D., Scurtu, A., Oane, M., Diplășu, C., Giubega, G., Călina, I., & Ticoș, C. M. (2019). Complementary dosimetry for a 6 MeV electron beam. *Results in Physics*, 14(February), 102377. <https://doi.org/10.1016/j.rinp.2019.102377>
- [7] Konigstein, T., Karger, O., Pretzler, G., Rosenzweig, J. B., & Hidding, B. (2012). Design considerations for the use of laser-plasma accelerators for advanced space radiation studies. *Journal of Plasma Physics*, 78(4), 383–391. <https://doi.org/10.1017/s0022377812000153>
- [8] Macchi, A., Borghesi, M., & Passoni, M. (2013). Ion acceleration by superintense laser-plasma interaction. *Reviews of Modern Physics*, 85(2), 751–793. <https://doi.org/10.1103/RevModPhys.85.751>
- [9] Tampo, M., Awano, S., Bolton, P. R., Kondo, K., Mima, K., Mori, Y., ... Kodama, R. (2010). Correlation between laser accelerated MeV proton and electron beams using simple fluid model for target normal sheath acceleration. *Physics of Plasmas*, 17(7). <https://doi.org/10.1063/1.3459063>
- [10] Danson, C., Hillier, D., Hopps, N., & Neely, D. (2015). Petawatt class lasers worldwide. *High Power Laser Science and Engineering*, 3(January). <https://doi.org/10.1017/hpl.2014.52>
- [11] Center for Advanced Laser Technologies (CETAL), Ultra-intense Lasers Laboratory -: <http://cetal.inflpr.ro/newsite/cetal-pw>

- [12] T. Asavei, M. Tomut, M. Bobeica, S. Aogaki, M.O. Cernaianu, M. Ganciu, S. Kar, G. Manda, N. Mocanu, L. Neagu, C. Postolache, D. Savu, D. Sutman, D. Vizman, D. Ursescu, S. Gales, N.V. Zamfir, "Materials in extreme environments for energy, accelerators and space applications at ELI-NP", *Romanian Reports in Physics*, **68**, Supplement, P. S275–S347 (2016)
- [13] Ganciu, M.; Groza, A.; Cramariuc, O.; Mihalcea, B.; Serbanescu, M.; Stancu, E.; Surmeian, A.; Butoi, B.; Dreghici, D.; Chiroasca, A.; Cramariuc, B.; Hardware and software methods for radiation resistance rising of the critical infrastructures. *Rom. Cyber Secur. J.* 2019, 1, 3–13.
- [14] A. Groza, M. Serbanescu, B. Butoi, E. Stancu, M. Straticiuc, I. Burducea, A. Balan, A. Chiroasca, B. Mihalcea, M. Ganciu, *Advances in Spectral Distribution Assessment of Laser Accelerated Protons using Multilayer CR-39 Detectors*, *Appl. Sci.* 2019, 9 (10), 2052; <https://doi.org/10.3390/app9102052>
- [15] G. Giubega, Proton acceleration in ultra-intense laser interaction with solid targets at CETAL-PW laser, Poster presentation, **WORKSHOP CETAL 2018**, <http://cetal.inflpr.ro/newsite/workshop>
- [16] Monsen Najafi, Ghazale Geraily, Alireza Shirazi, Mahbod Esfahani, Javad Teimouri, Analysis of Gafchromic EBT3 film calibration irradiated with gamma rays from different systems: Gamma Knife and Cobalt-60 unit, *Medical Dosimetry* 2017
- [17] <https://imagej.nih.gov/ij/docs/examples/calibration/>
- [18] <http://tomography.inflpr.ro/>
- [19] Hidding, B., Karger, O., Königstein, T., Pretzler, G., Manahan, G. G., McKenna, P., R. Gray, R. Wilson, S. M. Wiggins, G. H. Welsh, A. Beaton, P. Delinikolas, D. A. Jaroszynski, J. B. Rosenzweig, A. Karmakar, V. Ferlet-Cavrois, A. Costantino, M. Muschitiello, Daly, E. (2017) Laser-plasma-based Space Radiation Reproduction in the Laboratory. *Scientific Reports*, 7(February), 1–6. <https://doi.org/10.1038/srep42354>
- [20] J. Fuchs, P. Antici, E. d'Humieres, E. Lefebvre, M. Borghesi, E. Brambrink, C. A. Cecchetti, M. Kaluza, V. Malka, M. Manclossi, S. Meyroneinc, P. Mora, J. Schreiber, T. Toncian, H. Pepin, and P. Audebert (2006). Laser-driven proton scaling laws and new paths towards energy increase. *Nature Physics*, 2(1), 48–54. <https://doi.org/10.1038/nphys199>
- [21] <http://www.nap.edu/read/5540/chapter/1>
- [22] <http://srag.jsc.nasa.gov/spaceradiation/how/how.cfm#Support>
- [23] Jeong, T.W.; Singh, P.K.; Scullion, C.; Ahmed, H.; Hadjisolomou, P.; Jeon, C.; Yun, H.; Kakolee, K.F.; Borghesi, M.; Ter-Avetisyan, S. (2017). CR-39 track detector for multi-MeV ion spectroscopy. *Scientific Reports*, 7(1), 2–9. <https://doi.org/10.1038/s41598-017-02331-w>
- [24] Sinenian, N.; Rosenberg, M.J.; Manuel, M.; McDuffee, S.C.; Casey, D.T.; Zylstra, A.B.; Rinderknecht, H.G.; Johnson, M.G.; Séguin, F.H.; Frenje, J.A. (2014). Erratum: "The response of CR-39 nuclear track detector to 1–9 MeV protons" [*Rev. Sci. Instrum.* 82, 103303 (2011)]. *Review of Scientific Instruments*, 85(11), 119901. <https://doi.org/10.1063/1.4901071>
- [25] Zhou, D., Sullivan, O. D., Semones, E., Zapp, N., Wang, S., Liu, S., Zhang B., Ye Z., Reitz G., Berger T., Benton, E. R. (2011). Radiation of Cosmic Rays Measured on the International Space Station 1 Introduction 2 LET Spectrum Method 3 Matroshka Experiments. 6, 107–110. <https://doi.org/10.7529/ICRC2011/V06/1248>
- [26] M. Ganciu, M.-I. Piso, O. Stoican, B. Mihalcea, C. Diplasu, O. Marghitu, A. Julea, A. Surmeian, A. Groza, R. Dabu, I. Morjan, Application System and method for testing components, circuits and complex systems using synchronized and pulsed fluxes consisting of laser accelerated particles, Patent Application, WO201503061 A1, WO201503061A4
- [27] Narici, L., Casolino, M., Fino, L. Di, Larosa, M., Picozza, P., Rizzo, A., & Zaconté, V. (2017). Performances of Kevlar and Polyethylene as radiation shielding on-board the International Space Station in high latitude radiation environment. *Scientific Reports*, (March), 1–11. <https://doi.org/10.1038/s41598-017-01707-2>
- [28] S. Agostinelli, J. Allison, K. Amako, J. Apostolakis, H. Araujo, P. Arce, M. Asai, D. Axen, S. Banerjee, G. Barrant, F. Behner, L. Bellagamba, J. Boudreau, L. Broglia, A. Brunengo, H. Burkhardt, S. Chauvie, J. Chuma, R. Chytrcek, G. Cooperman, G. Cosmo, P. Degtyarenko, A. Dell'Acqua, G. Depaola, D. Dietrich, R. Enami, A. Feliciello, C. Ferguson, H. Fesefeldt, G. Folger, F. Foppiano, A. Forti,

- S. Garelli, S. Giani, R. Giannitrapani, D. Gibin, J.J. Gómez Cadenas, I. González, G. Gracia Abril, G. Greeniaus, W. Greiner, V. Grichine, A. Grossheim, S. Guatelli, P. Gumplinger, R. Hamatsu, K. Hashimoto, H. Hasui, A. Heikkinen, A. Howard, V. Ivanchenko, A. Johnson, F.W. Jones, J. Kallenbach, N. Kanaya, M. Kawabata, Y. Kawabata, M. Kawaguti, S. Kelner, P. Kent, A. Kimura, T. Kodama, R. Kokoulin, M. Kossov, H. Kurashige, E. Lamanna, T. Lampén, V. Lara, V. Lefebvre, F. Lei, M. Liendl, W. Lockman, F. Longo, S. Magni, M. Maire, E. Medernach, K. Minamimoto, P. Mora de Freitas, Y. Morita, K. Murakami, M. Nagamatu, R. Nartallo, P. Nieminen, T. Nishimura, K. Ohtsubo, M. Okamura, S. O'Neale, Y. Oohata, K. Paech, J. Perl, A. Pfeiffer, M.G. Pia, F. Ranjard, A. Rybin, S. Sadilov, E. Di Salvo, G. Santin, T. Sasaki, N. Savvas, Y. Sawada, S. Scherer, S. Sei, V. Sirotenko, D. Smith, N. Starkov, H. Stoecker, J. Sulkimo, M. Takahata, S. Tanaka, E. Tcherniaev, E. Safai Tehrani, M. Tropeano, P. Truscott, H. Uno, L. Urban, P. Urban, M. Verderi, A. Walkden, W. Wander, H. Weber, J.P. Wellisch, T. Wenaus, D.C. Williams, D. Wright, T. Yamada, H. Yoshida, D. Zschesche, Geant4—a simulation toolkit, *Nuclear Instruments and Methods in Physics Research Section A: Accelerators, Spectrometers, Detectors and Associated Equipment*, Volume 506, Issue 3, 2003, Pages 250-303, ISSN 0168-9002, [https://doi.org/10.1016/S0168-9002\(03\)01368-8](https://doi.org/10.1016/S0168-9002(03)01368-8).
- [29] J. Allison et al., "Geant4 developments and applications," in *IEEE Transactions on Nuclear Science*, vol. 53, no. 1, pp. 270-278, Feb. 2006. doi: 10.1109/TNS.2006.869826
- [30] J. Allison, K. Amako, J. Apostolakis, P. Arce, M. Asai, T. Aso, E. Bagli, A. Bagulya, S. Banerjee, G. Barrand, B.R. Beck, A.G. Bogdanov, D. Brandt, J.M.C. Brown, H. Burkhardt, Ph. Canal, D. Cano-Ott, S. Chauvie, K. Cho, G.A.P. Cirrone, G. Cooperman, M.A. Cortés-Giraldo, G. Cosmo, G. Cuttone, G. Depaola, L. Desorgher, X. Dong, A. Dotti, V.D. Elvira, G. Folger, Z. Francis, A. Galoyan, L. Garnier, M. Gayer, K.L. Genser, V.M. Grichine, S. Guatelli, P. Guèye, P. Gumplinger, A.S. Howard, I. Hrivnáčová, S. Hwang, S. Incerti, A. Ivanchenko, V.N. Ivanchenko, F.W. Jones, S.Y. Jun, P. Kaitaniemi, N. Karakatsanis, M. Karamitros, M. Kelsey, A. Kimura, T. Koi, H. Kurashige, A. Lechner, S.B. Lee, F. Longo, M. Maire, D. Mancusi, A. Mantero, E. Mendoza, B. Morgan, K. Murakami, T. Nikitina, L. Pandola, P. Paprocki, J. Perl, I. Petrović, M.G. Pia, W. Pokorski, J.M. Quesada, M. Raine, M.A. Reis, A. Ribon, A. Ristić Fira, F. Romano, G. Russo, G. Santin, T. Sasaki, D. Sawkey, J.I. Shin, I.I. Strakovsky, A. Taborda, S. Tanaka, B. Tomé, T. Toshito, H.N. Tran, P.R. Truscott, L. Urban, V. Uzhinsky, J.M. Verbeke, M. Verderi, B.L. Wendt, H. Wenzel, D.H. Wright, D.M. Wright, T. Yamashita, J. Yarba, H. Yoshida, Recent developments in Geant4, *Nuclear Instruments and Methods in Physics Research Section A: Accelerators, Spectrometers, Detectors and Associated Equipment*, Volume 835, 2016, Pages 186-225, ISSN 0168-9002, <https://doi.org/10.1016/j.nima.2016.06.125>.
- [31] Xiao, K. D., Zhou, C. T., Jiang, K., Yang, Y. C., Li, R., Zhang, H., ... He, X. T. (2018). Multidimensional effects on proton acceleration using high-power intense laser pulses. *Physics of Plasmas*, 25(2). <https://doi.org/10.1063/1.5003619>
- [32] Volpe, L., Fedosejevs, R., Gatti, G., Pérez-Hernández, J. A., Méndez, C., Apiñaniz, J., ... Roso, L. (2019). Generation of high energy laser-driven electron and proton sources with the 200 TW system VEGA 2 at the Centro de Lasers Pulsados. *High Power Laser Science and Engineering*, 7, 6–11. <https://doi.org/10.1017/hpl.2019.10>
- [33] Fuchs, J., Antici, P., D'Humières, E., Lefebvre, E., Borghesi, M., Brambrink, E., ... Audebert, P. (2006). Laser-driven proton scaling laws and new paths towards energy increase. *Nature Physics*, 2(1), 48–54. <https://doi.org/10.1038/nphys199>
- [34] T. Ersmark, Geant4 Monte Carlo Simulations of the International Space Station Radiation Environment, Doctoral Thesis KTH Fysik, Stockholm, Sweden 2006,
- [35] Shavers, M. (n.d.). Radiation Measurements and Shielding Analysis for ISS Low Earth Orbit and Exploratory Missions Instrumentation and Analysis Parameters for Ionizing Radiation Dosimetry. [http://www.iss-casis.org/files/CASIS\\_RFP\\_2013\\_3\\_Radiation\\_Measurements\\_and\\_Shielding\\_Analysis\\_for\\_ISS.pdf](http://www.iss-casis.org/files/CASIS_RFP_2013_3_Radiation_Measurements_and_Shielding_Analysis_for_ISS.pdf)